

# Difficulties in Predicting Vortex Breakdown Effects on a Rolling Delta Wing

Lars E. Ericsson\*  
Mountain View, California 94040

An analysis has been performed of the challenges encountered when trying to predict the unsteady aerodynamics associated with the breakdown of the leading-edge vortices on a 65-deg sharp-edged delta wing, describing roll oscillations around an axis inclined 30 deg to the freestream. It is shown that to produce a realistic prediction the mathematical model has to represent in a satisfactory manner the highly nonlinear, almost discontinuous steady and unsteady aerodynamic characteristics associated with the downstream travel of the vortex breakdown past the trailing edge on the leeward wing half at  $5 < |\phi| < 8$  deg.

## Nomenclature

$b$	= wingspan
$c$	= wing root chord
$C_\mu$	= blowing coefficient, Fig. 11
$C_{\mu m}$	= alternating blowing-suction coefficient at $fc/U = 1.3$ , Fig. 12
$f$	= oscillation frequency
$k$	= reduced frequency, $\omega b/2U_\infty$
$l$	= rolling moment: coefficient $C_l = l/(\rho_\infty U_\infty^2/2)Sb$
$P(t)$	= flow state parameter, $\phi(t)$ , $\dot{\phi}(t)$
$S$	= reference area, projected wing area
$t$	= time
$U$ , $U_\infty$	= freestream velocity
$x$	= axial body-fixed coordinate, Fig. 11
$\alpha$	= angle of attack
$\gamma$	= $\cos^{-1}(\cos \alpha \sin \Lambda)$
$\Delta t$	= time lag
$\Delta \phi$	= roll oscillation amplitude
$\Lambda$	= leading-edge sweep angle
$\xi$	= dimensionless $x$ coordinate, $x/c$
$\rho$	= air density
$\phi$	= roll angle
$\phi(0)$	= initial roll angle
$\omega$	= angular frequency

## Subscripts

$d$	= discontinuity
$sd$	= statically destabilizing
$V$	= vortex
$VB$	= vortex breakdown
$\infty$	= freestream conditions

## Differential Symbol

$\dot{\phi}$	= $\partial \phi / \partial t$
--------------	--------------------------------

## Introduction

THE unsteady aerodynamics of a sharp-edged 65-deg delta wing, describing high-rate/large-amplitude roll oscillations around the body axis at 30-deg flow inclination, have been shown to be surprisingly complex.<sup>1–4</sup> It was recently

demonstrated that the source of the complex, highly nonlinear vehicle dynamics is the presence of the critical flow states,<sup>5</sup> associated with the breakdown of the leading-edge vortices.<sup>6</sup> As an analysis of how to include agility considerations in the design of fighter aircraft<sup>7</sup> has concluded that torsional agility is most important, followed by axial and pitch agility, it is obviously important to be able to predict the unsteady aerodynamics of rapid roll maneuvers. This demands satisfactory prediction of the dynamic breakdown characteristics of leading-edge vortices on a rolling delta wing. Two attempts have been made to solve this challenging problem; first by Huang and Hanff,<sup>8</sup> using an analytic method, and later by Chaderjian and Schiff,<sup>9</sup> using a numerical method. In this article experimental results are analyzed to determine to what extent these theoretical methods can predict the dynamic effects of vortex breakdown on a rolling delta wing. It is found that neither method appears to provide an adequate simulation of the experimental results.

## Analysis

One has to start at the source, i.e., the prediction of the static vortex breakdown characteristics. At a first look, Fig. 1 appears satisfactory. However, further examination reveals important differences between prediction and experimental results. The analytic method<sup>8</sup> cannot predict the nonlinear data trend for one particular test, such as that performed either by Wentz and Kohlman<sup>10</sup> or by Payne<sup>11</sup> (Fig. 2). When comparing prediction with all available test data, as is done in Fig. 1, one easily can lose sight of important breakdown characteristics. This problem is illustrated by the test results<sup>12</sup> in Fig. 3.

One obvious problem with using data from tests in different facilities is the effects of different ground facility interference<sup>13–15</sup> and differences in Reynolds number and wind-tunnel turbulence.<sup>16,17</sup> When adding to this the significant effect of the cross-sectional leading-edge geometry,<sup>18</sup> one can appreciate the problem with the approach taken in Ref. 8, giving the prediction shown in Fig. 1, and illustrated in more detail in Fig. 2 for the 75-deg delta wing. Figure 2 shows how Ref. 8 underpredicts the experimentally observed rapidly increasing rate of the aft movement of the vortex breakdown with decreasing angle of attack when it passes downstream of midchord. It is true that the Wentz–Kohlman results<sup>10</sup> are flawed,<sup>19</sup> probably because of aeroelastic deflection of the thin plate models used. However, the Payne results<sup>11</sup> show a very similar deviation from the prediction.<sup>8</sup> The compilation of experimental data by Delery,<sup>20</sup> for a 70-deg delta wing (Fig. 4), shows a similar nonlinear data trend, represented by the solid line. The rate of downstream travel of the breakdown with decreasing angle of attack increases greatly for  $\xi_{VB} > 0.4$ .

Presented as Paper 94-1883 at the AIAA 12th Applied Aerodynamics Conference, Colorado Springs, CO, June 20–23, 1994; received July 14, 1994; revision received Nov. 22, 1995; accepted for publication Nov. 23, 1995. Copyright © 1995 by L. E. Ericsson. Published by the American Institute of Aeronautics and Astronautics, Inc., with permission.

\*Consulting Engineer. Fellow AIAA.

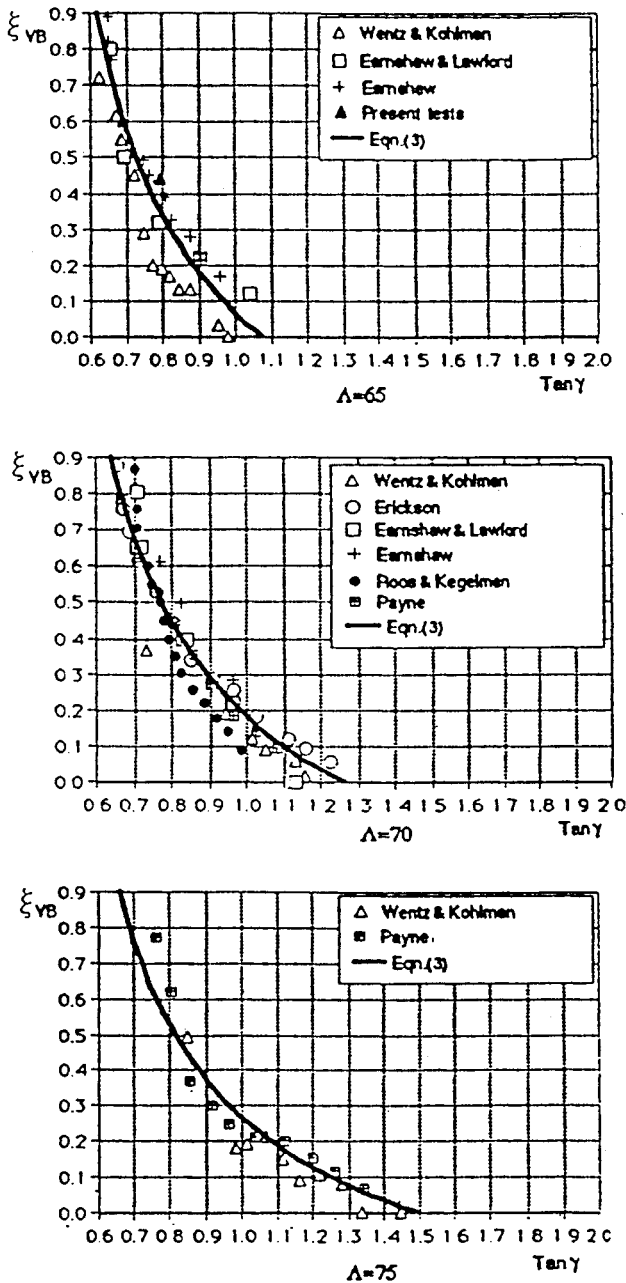


Fig. 1 Effect of leading-edge sweep on delta wing vortex breakdown.<sup>8</sup>

The nonlinear data trend in Fig. 4 was approximated as shown in Fig. 5 in the analysis in Refs. 3, 4, 6, and 21. Reference 6 illustrates that the breakdown travel will be equally nonlinear as a function of roll angle, using these idealized experimental results to produce Fig. 6. When accounting for the beveled leading edge of the 65-deg delta wing,<sup>1</sup> the effective angle of attack is less than the nominal value.<sup>18</sup> As Fig. 6b shows,  $\alpha(\phi) \approx \sigma$  for  $|\phi| < 10$  deg, a constant  $\alpha$  value,  $\alpha < 30$  deg, should be used (shown by the dashed line in Fig. 6a), indicating that if the leading-edge sweep is increased to approach  $\Lambda = 70$  deg on the rolling 65-deg delta wing, the vortex breakdown would more or less jump towards the trailing edge with further increase of the sweep angle. Figure 6b shows that a value of  $\Lambda = 69$  deg would be reached on the leeward wing half (in the lateral sense) when the roll angle is approaching the critical region  $5 < \phi < 8$  deg (Fig. 7), leading to the use in Ref. 6 of the idealized, discontinuous characteristics shown by a solid line in Fig. 7. In contrast to this emphasis on the effect of the critical state, the analysis in Ref. 8 gives a pre-

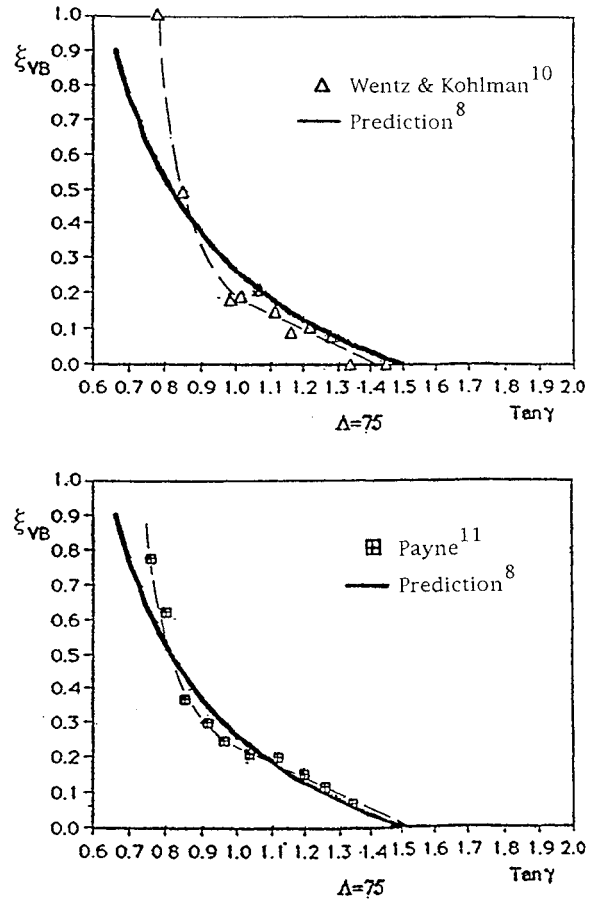


Fig. 2 Vortex breakdown on 75-deg delta wing.

diction that cannot capture the effect of the critical state, judging by the results in Fig. 8. The prediction in Ref. 9, through the use of a Navier-Stokes code, does show an effect of the critical state (Fig. 9). However, the agreement with the experimental results<sup>1</sup> needs to be better before prediction of the dynamic characteristics will be possible, as will be discussed.

There are two critical states for the 65-deg delta wing rolling around an axis inclined 30 deg.<sup>5,6</sup> The one that has been discussed so far is the loss of the vortex breakdown on the laterally leeward wing half, resulting in a sudden increase of the vortex-induced lift. This generates a statically destabilizing rolling moment trend that is initiated at  $|\phi| = \phi_{sd}$  and completed at  $|\phi| = \phi_d$  as the experiment rather than occurring instantly at  $|\phi| = \phi_d$ , as assumed in the idealized case (Fig. 7). As discussed in Refs. 5 and 6, at some roll angle  $|\phi| \approx 10$ -deg vortex breakdown on the laterally windward wing half reaches the apex. This constitutes the second critical state. In the present case of  $\sigma = 30$  deg, the effect of this critical state is insignificant. However, at  $\sigma = 35$  deg it is the dominant critical state, generating most of the experimentally observed<sup>22</sup> highly nonlinear, statically destabilizing variation of the rolling moment around  $\phi = 0$ .

### Dynamic Vortex Breakdown

Figure 10 shows a comparison of the predicted<sup>8</sup> and experimental<sup>1</sup> breakdown locations on the 65-deg delta wing, describing roll oscillations of 33-deg amplitude around  $\phi = 0$  at the reduced frequencies  $k = 0.02$  and  $k = 0.20$ . It is at first surprising that the agreement between prediction and experiment is better for  $k = 0.20$  than for  $k = 0.02$ . However, the good agreement for  $k = 0.20$  is to be expected as the prediction uses experimental results<sup>8</sup> for the roll-rate-induced camber effect<sup>4</sup> measured on a model representing  $k = 0.20$ . One reason for the poor agreement for  $k = 0.02$  in Fig. 10 is the assumption

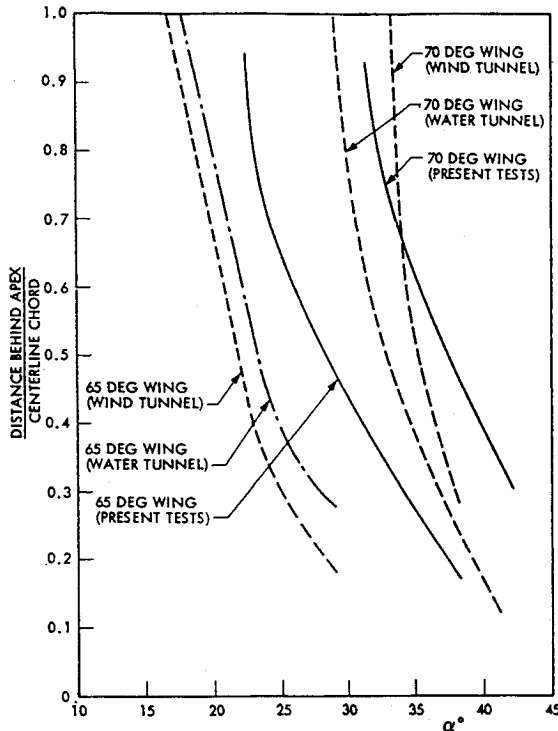


Fig. 3 Vortex breakdown on 65- and 70-deg delta wings.<sup>12</sup>

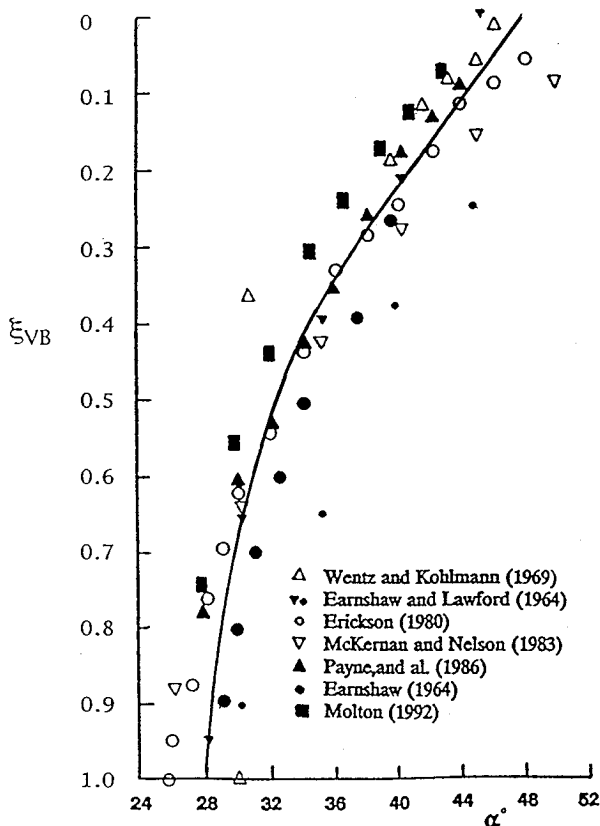


Fig. 4 Compilation of experimental results for vortex breakdown on 70-deg delta wing.<sup>20</sup>

in Ref. 8 that the roll-rate-induced camber effect would be only a tenth as large for  $k = 0.02$  as for  $k = 0.20$ , i.e., the camber effect was assumed to vary linearly with  $k$ . Because of the presence of the critical state and the associated highly nonlinear flow characteristics, it happens that the camber effect is almost of the same magnitude at  $k = 0.02$  as at  $k = 0.20$ . The

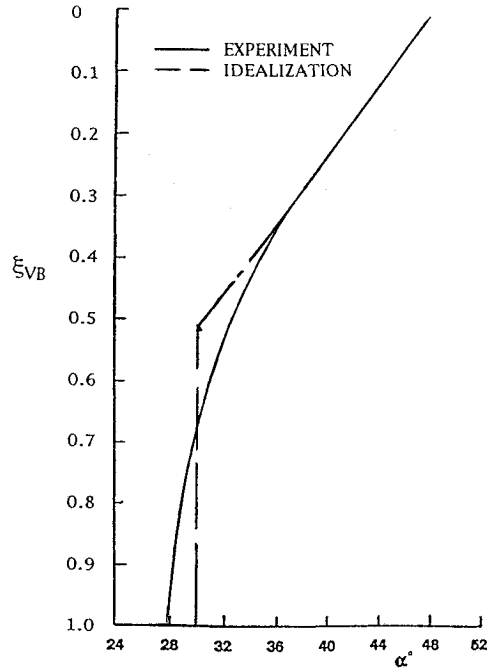


Fig. 5 Idealization of experimental data trend for vortex breakdown on 70-deg delta wing.

camber effect becomes extremely large when the breakdown approaches the critical position, the knee of the idealized characteristics in Fig. 6a for  $\Lambda \approx 69$  deg. Note that the rate-induced camber effect is expected to increase with the roll angle in the same rapid manner as the static  $\alpha$  effect increases when the knee is approached in Fig. 6a. (In reality the knee has a much more rounded shape than in the idealization.)

Recent experimental results for a 75-deg delta wing<sup>23</sup> (Figs. 11 and 12) illustrate the changing breakdown behavior when the knee is approached. Without blowing, the breakdown was located at 29% chord, which places it close to the knee for the 75-deg delta wing in Fig. 6a. Consequently, the nonlinear beneficial effect of tangential leading-edge blowing, shown in Figs. 11 and 12, is to be expected. To quote the authors in regard to Fig. 11: "Considering the overall response of the vortex, it is evident that the downstream movement of vortex breakdown does not occur in a smooth, continuous fashion. Little change occurs over the interval  $0 \leq tU/c \leq 0.8$ , whereas a very substantial alteration occurs over the time interval  $0.8 \leq tU/c \leq 1.7$ ." The long time delay for the vortex breakdown to react to the effect of blowing is very similar to the observed time delay in realizing the effect of pitch-rate-induced camber.<sup>24</sup> One expects the effect of roll-rate-induced camber to be associated with similarly large time-lag effects. Figure 12 shows that the breakdown-delaying effect of tangential leading-edge blowing-suction is saturated very fast. The same is likely to be the case for the roll-rate-induced camber effect.

In Fig. 13 the experimental static ( $\bullet$ ) and dynamic ( $\circ$ ) vortex breakdown results<sup>8</sup> are shown for the starboard wing half of the 65-deg delta wing.<sup>8</sup> Also shown is the effect of a constant time lag  $\Delta t$ . According to the analysis in Ref. 25, the time history effects can be represented by a lumped time-lag effect, as long as the axial extent of the vehicle is less than one-quarter wavelength of the oscillation, i.e.,  $\omega c/U_\infty < \pi/2$ . That is,  $k < 0.73$  in the present case, a condition well satisfied by the experiments discussed in Refs. 1 and 8. For  $|\phi| \leq 10$  deg, the angular lag corresponding to the time lag is  $\Delta\phi = \phi\Delta t \approx \phi(0)\Delta t$ , considering that  $0.95 \leq \phi(\phi)/\phi(0) \leq 1.00$  for the 33-deg oscillation amplitude. However, for  $|\phi| > 10$  deg, one finds that instead of being less than  $\phi(0)\Delta t$ , the measured lag  $\Delta\phi$  is significantly larger than the constant angular lag  $\Delta\phi$ . The difference between the estimated time-lag effect and the experi-

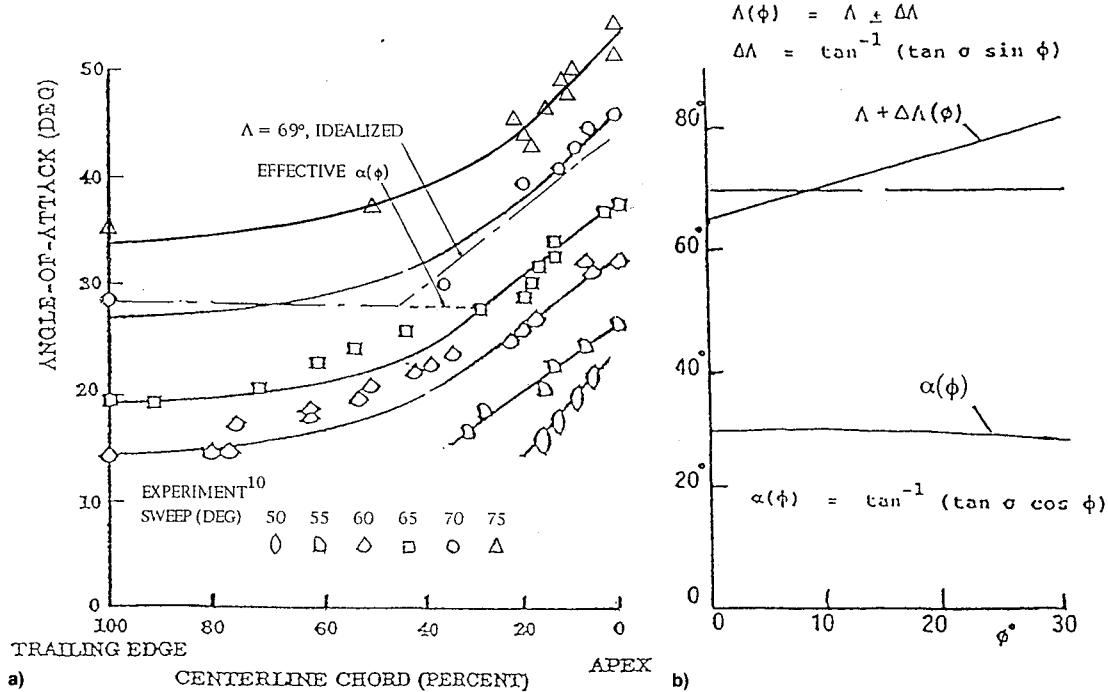


Fig. 6 Static delta wing vortex breakdown characteristics: a) breakdown location on sharp-edged delta wings and b) effect of roll angle on effective leading-edge sweep.<sup>6</sup>

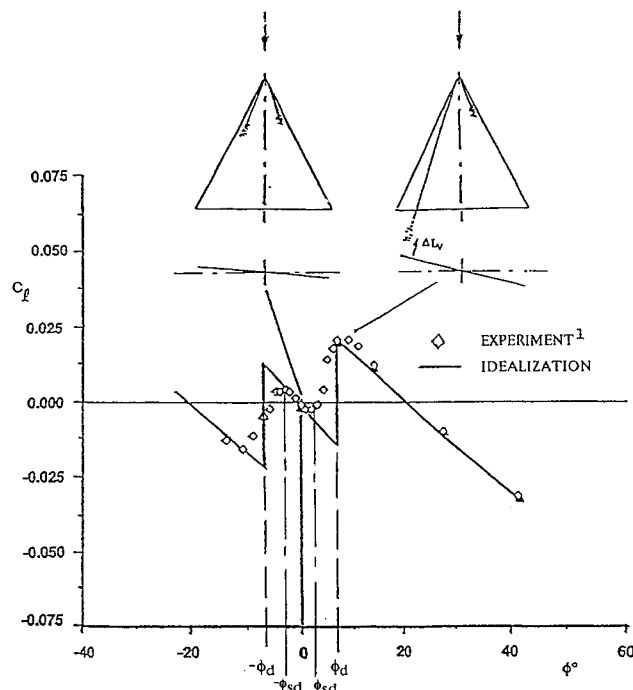


Fig. 7 Idealized, discontinuous  $C_l(\phi)$  characteristics of 65-deg delta wing at 30 deg inclination of the roll axis.<sup>4</sup>

mental results is caused by the effect of the roll-rate-induced camber.<sup>3,4,6</sup> During the upstroke,  $\phi < 0$  in Fig. 13, this dynamic camber effect promotes vortex breakdown, as illustrated by the inset sketches at  $\phi = -10$  deg. Note that the dynamic camber effect cannot be large when static vortex breakdown occurs forward of 20% chord, where the forward movement of the breakdown with increasing angle of attack has slowed down considerably (Fig. 6a). That is the logic behind the placement of the curve representing the effect of a constant time lag for  $\phi < 0$ . During the downstroke,  $\phi > 0$ , the roll-rate-induced camber delays vortex breakdown, as illustrated in the inset sketches at  $\phi = 10$  deg in Fig. 13. Such a delay is also indi-

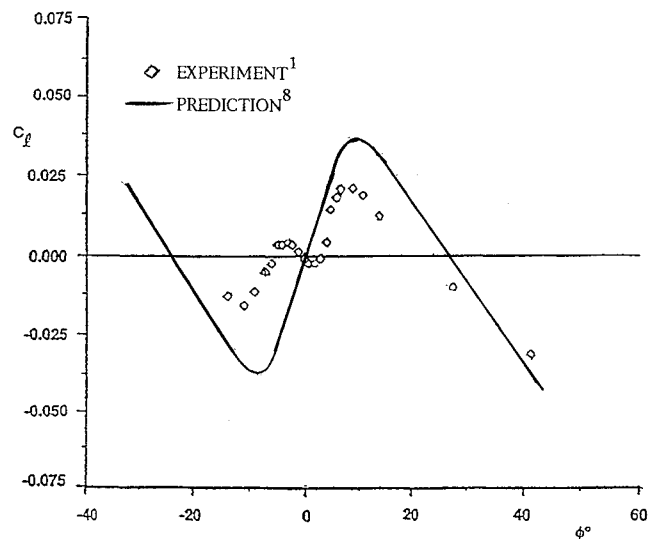


Fig. 8 Comparison between predicted and experimental  $C_l(\phi)$  characteristics for 65-deg delta wing.<sup>8</sup>

cated by the experimental results, when they are compared with the dash-dot curve representing the effect of a constant time lag. That the camber-induced delay of vortex breakdown at  $\phi > 0$  is of less magnitude than the camber-induced promotion at  $\phi < 0$  is to be expected, because it is easier to promote flow separation than to delay it.

It is obvious that the rapid, almost jumpwise movement of the breakdown location from midchord to the trailing edge, shown in Figs. 4-7, has to be modeled. The roll-rate-induced camber effect triggers this jumpwise movement of vortex breakdown, thereby having a dominating effect on the free-to-roll dynamics<sup>5,6</sup> (Fig. 14).

### Time History Effects

In Fig. 14 the difference in effective roll-rate-induced cambers, including the effect of time lag, is illustrated by the inset sketches. The effective roll angle and roll rate determining the delta wing characteristics at time  $t$ ,  $P(t)$ , are those generated

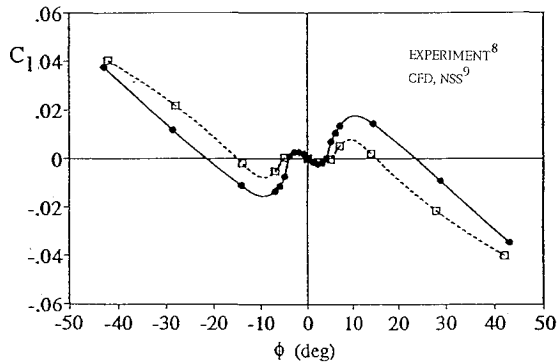


Fig. 9 Prediction of experimental  $C_l(\phi)$  characteristics using a Navier-Stokes code.<sup>9</sup>

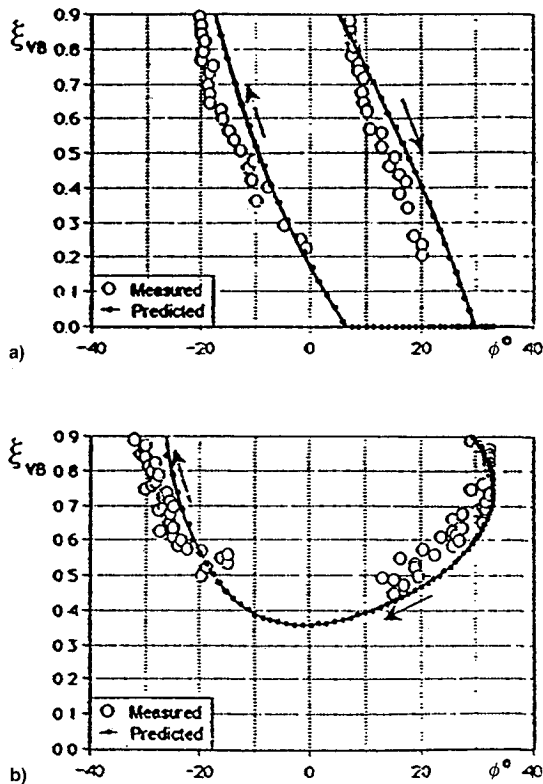


Fig. 10 Comparison of predicted and experimental vortex breakdown position on a 65-deg delta wing during 33-deg roll oscillations.<sup>8</sup>  $k = a) 0.02$  and  $b) 0.20$ .

at  $t - \Delta t$ , i.e.,  $P(t - \Delta t)$ . For simplicity, it is assumed in the discussion to follow that the time lag is the same for the effects of roll angle and roll rate. Figure 14 shows that for the  $\phi(0) = -66^\circ$  release the effective roll rate at  $t - \Delta t$  is of lesser magnitude, but of the same sign, as the one at  $t$ , and the effective roll angle is substantially to the left of  $\phi = -5^\circ$ , resulting in the vortex geometry illustrated in the sketch. That is, the vortex burst has left the leeside wing half and has moved close to the apex on the windward side. Thus, the dynamic effect is to generate a rolling-moment increment  $\Delta C_l < 0$ . Note that the effect of the roll-rate-induced camber on the unburst vortex contributes also to this negative rolling-moment increment.<sup>26</sup> In contrast, in the case of the  $\phi(0) = 57^\circ$  release, the effective roll rate  $\phi(t - \Delta t)$  is of the opposite sign relative to the instantaneous roll rate at  $t$ . The effective roll angle  $\phi(t - \Delta t)$  is essentially the same as the instantaneous angle  $\phi(t)$ . The result is that the vortex breakdown moves upstream on the leeside wing half rather than downstream, as in the case of the  $\phi(0) = -66^\circ$  release, and moves down-



Fig. 11 Dye visualization of the effect of  $C_{\mu} = 0.036$  on vortex breakdown on a 75-deg delta wing at  $\alpha = 54^\circ$  (Ref. 23).

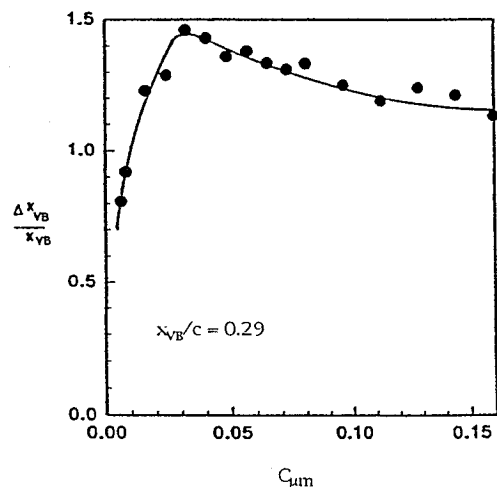


Fig. 12 Effect of  $C_{\mu}$  on the vortex breakdown of 75-deg delta wing.<sup>23</sup>

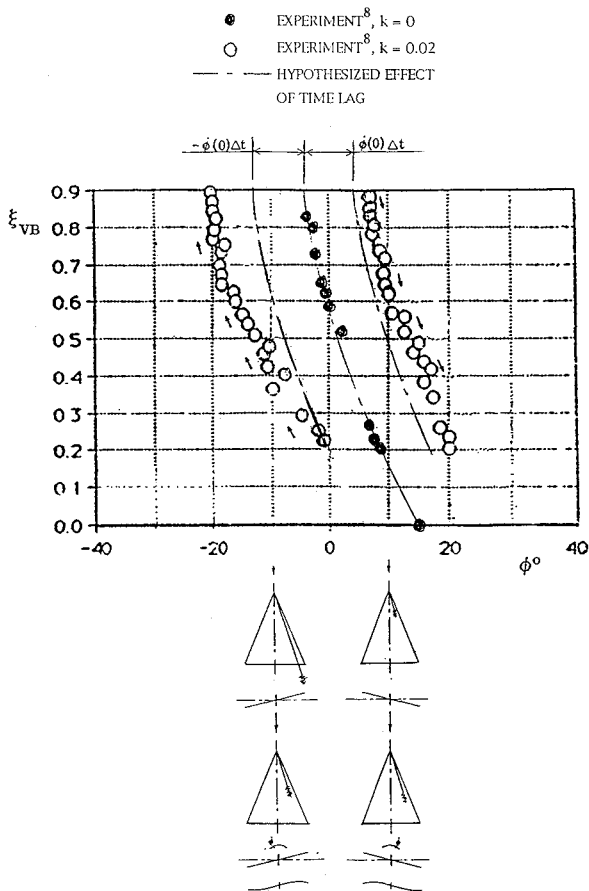


Fig. 13 Hypothesized effect of time lag on vortex breakdown location,  $k = 0.02$  and  $\Delta\phi = 33$  deg.

stream on the windward wing half. Thus, the dynamic effect is to generate a rolling moment increment  $\Delta C_l > 0$ . With the help of the flow physics just described one can understand why the  $\phi(0) = -66$ -deg release converges to the  $\phi \approx 0$  trim point, whereas the  $\phi(0) = 57$ -deg release is pushed away from that trim point.

The experimental results<sup>27</sup> in Fig. 15 illustrate the dominant effect of the roll-rate-induced camber. As called out<sup>27</sup> in the original Fig. 15, for the 5-deg roll amplitude, the authors did not expect to encounter any critical-state effects, as they occurred in static tests only for  $|\phi| > 5$  deg. Thus, the authors expected the  $C_l(\phi)$  characteristics to be similar to those in Fig. 16, where no critical states are traversed by the oscillation, as  $\phi > 20$  deg. Instead of the insignificant effects of roll rate exhibited in Fig. 16, Fig. 15 shows the effects to be large. The reason for this difference in the rolling moment variation with  $\phi(t)$  is, of course, that in Fig. 16 the oscillations never approached any critical state,<sup>5,6</sup> in contrast to the case shown in Fig. 16, where the oscillations approach the critical-state region,  $5 < |\phi| < 8$  deg. Thus, the roll-rate-induced camber generated at  $P(t)$  by the large roll rate at  $P(t - \Delta t)$  can twist the delta wing enough to encounter the critical state in Fig. 15, but not in Fig. 16. Examining the results in Fig. 15 closer, one finds that they provide further support for the hypothesized effect of time-lagged, roll-rate-induced camber.

In Fig. 15 the effect of  $k = 0.02$  is examined in detail. The inset sketches show, as in Fig. 14, how the roll-rate-induced camber generates the measured moment increments  $\Delta C_l$ . Because of the time-lag effect, the induced camber acting at  $P(t)$  was generated a time increment  $\Delta t$  earlier, at  $P(t - \Delta t)$ , close to  $\phi = 0$ , where the roll rate is near its maximum magnitude. The square-corner shape of the  $C_l(\phi)$  loop indicates how powerful the roll-rate-induced camber effect is. For it to be insignificant,

resulting in  $\Delta C_l \approx 0$  at the intersection of dynamic and static  $C_l$  curves, the roll rate at  $t - \Delta t$  has to be close to zero, i.e.,  $P(t - \Delta t)$  has to be close to the ends of the loop. For  $k = 0.02$ , the corresponding  $P(t)$  does not occur far from  $P(t - \Delta t)$ , less than 1 deg from the ends of the loop (Fig. 15). For  $k = 0.14$ , however, the time-lag effect is much larger, and  $\Delta C_l \approx 0$  is encountered at  $|\phi| < 2$  deg, more than 3 deg away from the ends of the loop (Fig. 17). This accounts for the rotation of the loops for increasing  $k$  (Fig. 17). Another observation to be made is that not only is the roll-rate-induced camber effect not larger for  $k = 0.14$  than for  $k = 0.02$ , because of the saturation of the rate-induced camber effect discussed earlier, it is actually smaller, judging by the  $C_l$  separation between upstroke and downstroke branches of the  $C_l$  loops in Fig. 17. The reason for this is the effect of time lag on the rate-induced camber. As illustrated by the results in Fig. 17,  $\Delta C_l = 0$  is reached 3 deg from the ends of the loops for  $k = 0.14$ , at  $|\phi| \approx 2$  deg, where the static  $C_l$  is of much lesser magnitude than at  $|\phi| > 4$  deg, where  $\Delta C_l = 0$  for  $k = 0.02$ .

Another consequence of this large time-lag effect is that the maximum and minimum  $\Delta C_l$ , obtained at  $P(t)$  when  $P(t - \Delta t)$  is located at  $\phi = 0$  (Fig. 15), is farther from  $\phi = 0$  for  $k = 0.14$  than for  $k = 0.02$  (Fig. 17). As a consequence, the maximum and minimum  $C_l$  values will occur closer to the ends of the loop for increasing  $k$ . More important is to observe that the enclosed area of the loop for  $k = 0.14$  is smaller than for  $k = 0.02$ . That is, instead of being seven times larger, as would be the case for linear aerodynamics, the damping in the present highly nonlinear case is actually smaller for  $k = 0.14$  than for

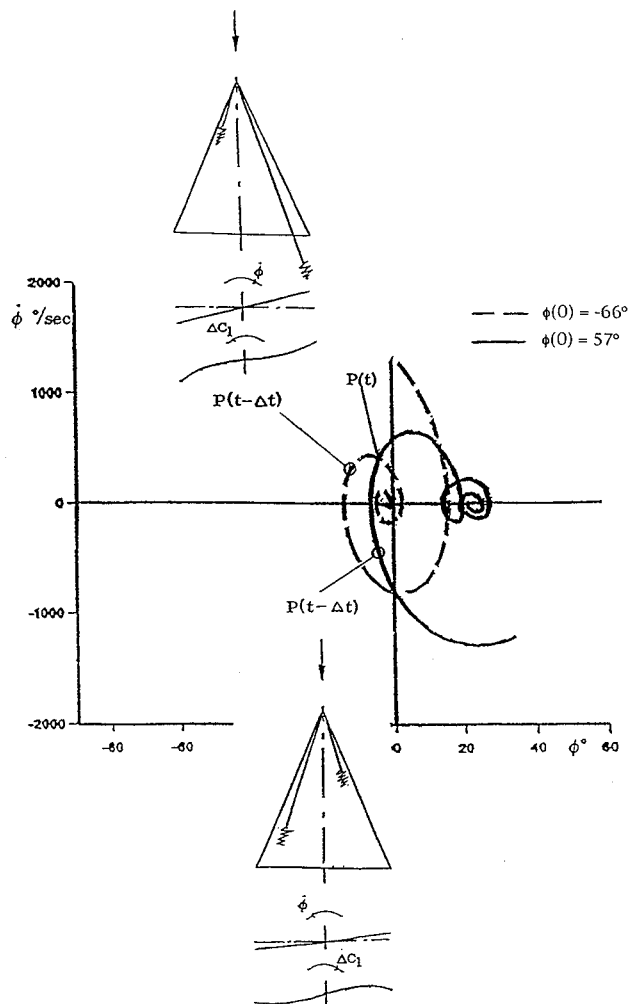


Fig. 14 Flow physics behind the observed phase plane characteristics of free-to-roll motions of 65-deg delta wing.<sup>6</sup>

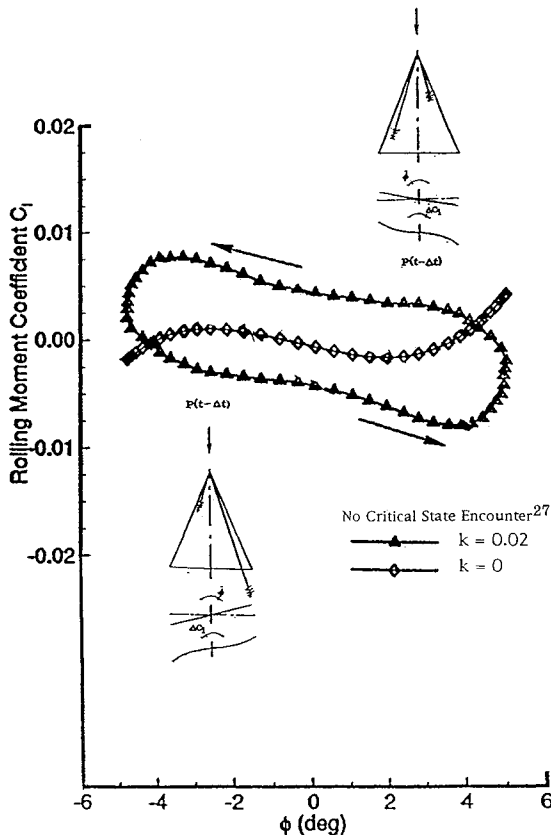


Fig. 15 Flow physics behind the observed  $C_l(\phi)$  characteristics of 65-deg delta wing for  $k = 0.02$ ,  $|\phi| \leq 5$  deg.

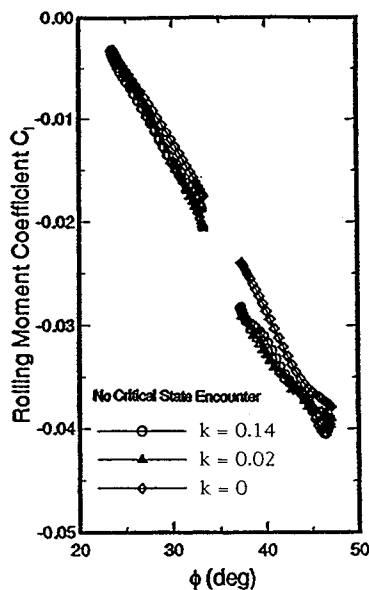


Fig. 16 Dynamic  $C_l(\phi)$  characteristics of 65-deg delta wing at  $\phi \geq 23$  deg (Ref. 27).

$k = 0.02$ . To predict the characteristics in Fig. 17 is still beyond presently existing theoretical capability. From conversations with Tobak,<sup>28</sup> the present author has drawn the conclusion that if the prediction of the static vortex breakdown characteristics is improved, through semiempirical means if needed, the analytic method of Ref. 8 could be developed further to provide reliable prediction of the vortex breakdown characteristics on a rolling delta wing.

As pointed out by Huang,<sup>29</sup> the difference between the dynamic characteristics for  $k = 0.02$  and  $0.14$  in Fig. 17 cannot

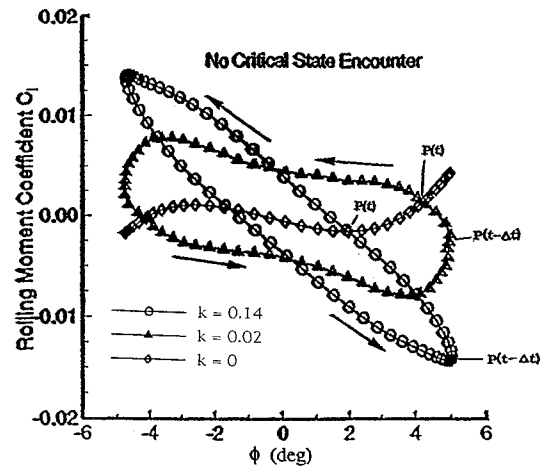


Fig. 17  $C_l(\phi)$  characteristics of 65-deg delta wing at  $|\phi| \leq 5$  deg (Ref. 27).

be explained solely by considering the time-lagged effect of the elimination of the roll-rate-induced camber at  $P(t - \Delta t)$ . Likewise, it is difficult to see how the roll-rate-induced camber by itself can explain the fact that the loop-area is larger for  $k = 0.02$  than for  $k = 0.14$ , even in the presence of the saturation of the rate-induced camber effect. It can be concluded that both roll-angle and roll-rate time histories must play important roles. More research is obviously needed before a reliable prediction method can be developed.

## Conclusions

An analysis of existing theoretical and experimental results for a 65-deg sharp-edged delta wing, describing rapid, large-amplitude roll oscillations around an axis inclined 30 deg to the freestream, has led to the following conclusions.

- 1) The extremely large effect of roll rate on vortex breakdown dynamics observed in experiments has so far defied theoretical prediction.
- 2) A careful examination of experimental results indicates that the difficulty is presented by the fact that the large effect of roll-rate-induced camber is highly nonlinear and associated with significant time history effects.
- 3) As the flow physics become better understood it will be possible to develop means for satisfactory prediction of the effect of vortex breakdown on rolling delta wings at high angles of attack, a necessity for successful design of high-agility aircraft.

## References

- <sup>1</sup>Hanff, E. S., and Jenkins, S. B., "Large-Amplitude High-Rate Roll Experiments on a Delta and Double Delta Wing," AIAA Paper 90-0224, Jan. 1990.
- <sup>2</sup>Hanff, E. S., and Ericsson, L. E., "Multiple Roll Attractors of a Delta Wing at High Incidence," CP-494, AGARD, July 1991 (Paper 31).
- <sup>3</sup>Ericsson, L. E., and Hanff, E. S., "Unique High-Alpha Roll Dynamics of a Sharp-Edged 65-Deg Delta Wing," *Journal of Aircraft*, Vol. 31, No. 3, 1994, pp. 520-525.
- <sup>4</sup>Ericsson, L. E., and Hanff, E. S., "Further Analysis of High-Rate Rolling Experiments of a 65-Deg Delta Wing," *Journal of Aircraft*, Vol. 31, No. 6, 1994, pp. 1350-1357.
- <sup>5</sup>Jenkins, J. E., Myatt, J. H., and Hanff, E. S., "Body-Axis Rolling Motion Critical States of a 65-Degree Delta Wing," AIAA Paper 93-0621, Jan. 1993.
- <sup>6</sup>Ericsson, L. E., "Flow Physics of Critical States for Rolling Delta Wings," *Journal of Aircraft*, Vol. 32, No. 3, 1995, pp. 603-610.
- <sup>7</sup>Skow, A. M., "Agility as a Contributor to Design Balance," *Journal of Aircraft*, Vol. 29, No. 1, 1992, pp. 34-46.
- <sup>8</sup>Huang, X. Z., and Hanff, E. S., "Prediction of Leading-Edge Vortex Breakdown on a Delta Wing Oscillating in Roll," AIAA Paper 92-2677, June 1992.

<sup>9</sup>Chaderjian, N. M., and Schiff, L. B., "Navier Stokes Prediction of Large-Amplitude Forced and Free-to Roll Delta Wing Oscillations," AIAA Paper 94-1884, June 1994.

<sup>10</sup>Wentz, W. H., and Kohlman, D. L., "Vortex Breakdown on Slender Sharp-Edged Delta Wings," *Journal of Aircraft*, Vol. 8, No. 3, 1971, pp. 156-161.

<sup>11</sup>Payne, F. M., "The Structure of Leading-Edge Vortex Flows Including Vortex Breakdown," Ph.D. Dissertation, Univ. of Notre Dame, Notre Dame, IN, May 1987.

<sup>12</sup>Earnshaw, P. B., "Measurements of Vortex-Breakdown Position at Low Speed on a Series of Sharp-Edged Symmetrical Models," Aeronautical Research Council CP 828, England, UK, 1965.

<sup>13</sup>Ericsson, L. E., and Reding, J. P., "Dynamic Support Interference in High-Alpha Testing," *Journal of Aircraft*, Vol. 23, No. 12, 1986, pp. 889-896.

<sup>14</sup>Ericsson, L. E., "Another Look at High-Alpha Support Interference," *Journal of Aircraft*, Vol. 28, No. 5, 1991, pp. 584-591.

<sup>15</sup>Beyers, M. E., and Ericsson, L. E., "Ground Facility Interference on Aircraft Configurations with Separated Flow," *Journal of Aircraft*, Vol. 30, No. 5, 1993, pp. 682-688.

<sup>16</sup>Ericsson, L. E., "Reflections Regarding Recent Rotary Rig Results," *Journal of Aircraft*, Vol. 24, No. 1, 1987, pp. 25-30.

<sup>17</sup>Ericsson, L. E., "Effects of Transition on Wind Tunnel Simulation of Vehicle Dynamics," *Progress in Aerospace Sciences*, Vol. 27, 1990, pp. 121-144.

<sup>18</sup>Ericsson, L. E., and King, H. H. C., "Effect of Leading-Edge Cross-Sectional Geometry on Slender Wing Unsteady Aerodynamics," *Journal of Aircraft*, Vol. 30, No. 5, 1993, pp. 793-795.

<sup>19</sup>Lowson, M. V., and Riley, A. J., "Vortex Breakdown Control by Delta Wing Geometry," *Journal of Aircraft*, Vol. 32, No. 4, 1995, pp. 832-838.

<sup>20</sup>Delery, J. M., "Aspects of Vortex Breakdown," *Progress in Aerospace Sciences*, Vol. 30, 1994, pp. 1-59.

<sup>21</sup>Ericsson, L. E., "Analysis of Wind-Tunnel Data Obtained in High-Rate Rolling Experiments with Slender Delta Wings," Inst. for Aerospace Research, CR-14, National Research Council, Ottawa, ON, Canada, Aug. 1991.

<sup>22</sup>Huang, X. Z., and Hanff, E. S., "Leading-Edge Vortex Behavior and Surface Flow Topology," AIAA Atmospheric Flight Mechanics Conf., Session AFM-16, Baltimore, MD, Aug. 1995.

<sup>23</sup>Gu, W., Robinson, O., and Rockwell, D., "Control of Vortices on a Delta Wing by Leading-Edge Injection," *AIAA Journal*, Vol. 31, No. 7, 1993, pp. 1177-1186.

<sup>24</sup>Ericsson, L. E., "Delta Wing Vortex Breakdown Dynamics," AIAA Paper 95-0367, Jan. 1995.

<sup>25</sup>Ericsson, L. E., and Reding, J. P., "Fluid Dynamics of Unsteady Separated Flow, Part II, Lifting Surfaces," *Progress in Aerospace Sciences*, Vol. 24, 1987, pp. 249-356.

<sup>26</sup>Ericsson, L. E., and King, H. H. C., "Rapid Prediction of High-Alpha Unsteady Aerodynamics of Slender-Wing Aircraft," *Journal of Aircraft*, Vol. 29, No. 1, 1992, pp. 85-92.

<sup>27</sup>Hsia, A. H., Myatt, J. H., and Jenkins, J. E., "Nonlinear and Unsteady Aerodynamic Responses of a Rolling 65-Degree Delta Wing," AIAA Paper 93-3682, Aug. 1993.

<sup>28</sup>Tobak, M., private communication, Nov. 1995.

<sup>29</sup>Huang, X. Z., private communication, Oct. 1995.

*Recommended Reading from Progress in Astronautics and Aeronautics*

# UNSTEADY TRANSONIC AERODYNAMICS

David Nixon, editor



1989, 385 pp, illus, Hardback  
ISBN 0-930403-52-5  
AIAA Members \$52.95  
Nonmembers \$69.95  
Order #: V-120 (830)

Unsteady transonic aerodynamics is a field with many differences from its counterpart, steady aerodynamics. The first volume of its kind, this timely text presents eight chapters on Physical Phenomena Associated with Unsteady Transonic Flows; Basic Equations for Unsteady Transonic Flow; Practical Problems: Airplanes; Basic Numerical Methods; Computational Methods for Unsteady Transonic Flow; Application of Transonic Flow Analysis to Helicopter Rotor Problems; Unsteady Aerodynamics for Turbomachinery Aeroelastic Applications; and Alternative Methods for Modeling Unsteady Transonic Flows. Includes more than 470 references, 180 figures, and 425 equations.

Place your order today! Call 1-800/682-AIAA



American Institute of Aeronautics and Astronautics

Publications Customer Service, 9 Jay Gould Ct., P.O. Box 753, Waldorf, MD 20604  
FAX 301/843-0159 Phone 1-800/682-2422 8 a.m. - 5 p.m. Eastern

Sales Tax: CA residents, 8.25%; DC, 6%. For shipping and handling add \$4.75 for 1-4 books (call for rates for higher quantities). Orders under \$100.00 must be prepaid. Foreign orders must be prepaid and include a \$20.00 postal surcharge. Please allow 4 weeks for delivery. Prices are subject to change without notice. Returns will be accepted within 30 days. Non-U.S. residents are responsible for payment of any taxes required by their government.